RSC Advances

ROYAL SOCIETY OF CHEMISTRY

www.rsc.org/advances

A graphical and textual abstract for the Table of contents entry

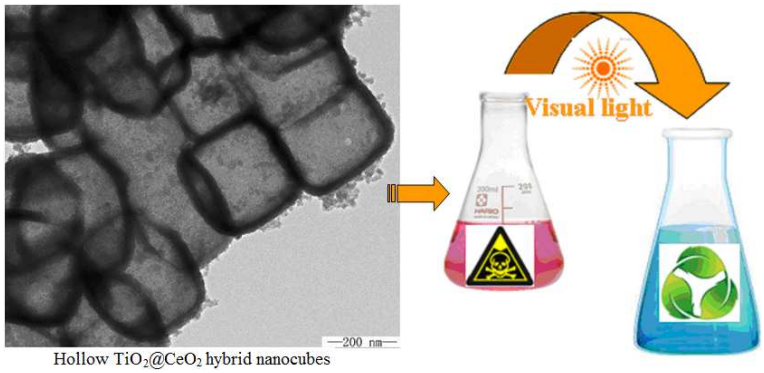

Hollow TiO_2@CeO_2 hybrid nanocubes

Hollow TiO_2@CeO_2 hybrid nanocubes are fabricated through a fast simultaneously coordinating etching and precipitation reactions. The intrinsic hollow cubic nature as well as the heterojunction effect of the unique nanostructures contributes greatly to the enhanced performance for photocatalytic detoxification of cyanide.

Journal Name

RSCPublishing

ARTICLE

Hierarchical hollow TiO_2@CeO_2 nanocube heterostructures for photocatalytic detoxification of cyanide

suCite this: DOI: 10.1039/xoxxoooooox

Yongjun Liu, Tingting Li, Weiwei Chen, Yuanyuan Guo, Lixiang Liu, Hong Guo*

Received ooth January 2012,
Accepted ooth January 2012

DOI: 10.1039/xoxxoooooox

www.rsc.org/

A facile generic strategy is employed to prepare hierarchical hollow TiO_2@CeO_2 nanocubes via a fast simultaneously coordinating etching and precipitation reactions. The intrinsic hollow cubic nature as well as the heterojunction effect of the unique nanostructures contributes greatly to the enhanced performance for photocatalytic detoxification of cyanide.

Numerous efforts have been made to develop highly effective photocatalysts for the photodecomposition of waterborne contaminants such as organic dye. However, reports on visible light photocatalytic mineralization of cyanide are quite few. In fact, the highly toxic cyanides are extensive present in effluent waters of several industries especially in electroplating, blast furnaces, coke producing plants, and precious-metals mining operations.[1-3] The alkaline chlorination is the best available proven technique.[4-6] Unfortunately, it may result in formation of highly toxic cyanogen chloride gas. Many efforts are used semiconductor photocatalysis to utilize solar energy for photocatalytic oxidation of cyanide with ultraviolet light, such as ZnO and TiO_2 materials.[7-11] Unfortunately, the wide band gap of these materials limits its light absorption only to the UV light range, while reports on visible light photocatalytic mineralization of cyanide are quite few. The main difficulties are as follows. To avoid volatilization of free CN^{-1}, the reaction must be stable in a highly alkaline basic medium because the value of pKa of HCN is ca. 9.3. The carbon in the CN^{-1} is more strongly bound to nitrogen than that with atoms in dye molecules, and thus the adsorption of the CN^{-1} on the photocatalytic surface becomes more difficulty with the increase of negative charge. So, photocatalytic removal of cyanide under visible light is still a great challenge. To solve these problems, designing and regulating coupled semiconductor heterojunction with matching band potentials has been proved as one of the most effective approaches to enhance photocatalytic activity because of the improved charge separation, increased charge carrier lifetime, and enhanced interfacial charge transfer efficiency from catalyst to adsorbed substrate.[12-15] For example, Bi_2WO_6 based hybrid materials and CeO_2/TiO_2 nanobelt heterostructures show enhanced photocatalytic performance.[16,17] Pd-$CoFeO_2$-GE composite nanosheets catalysts exhibit a remarkable catalytic activity towards the reduction of 4-nitrophenol by sodium borohydride at room temperature.[18] Sol-gel-prepared CeO_2/TiO_2 film and CeO_2/TiO_2 nanoparticles prepared by mechanical grinding, solvothermal, and hydrothermal methods have been shown to degrade dye photocatalytically under visible light.[19,20] Furthermore, accurate designing molecular architecture of nano/micro-semiconductors can effectively improve their photocatalytic performance, and thus it is another important approach to enhance the photocatalytic active. As one type of promising architectures, hollow nanostructure with well-defined interior voids, a large surface area, abundant active sites for reaction compared with that of solid counterparts of the same size, have attracted much attention and been investigated for a long time.[21-23] For instance, TiO_2 based hollow materials with different size and morphologies have enhanced photocatalytic activity.[7,10-11] Our previous prepared yolk-shell Ag@TiO_2 and Pd@CeO_2 materials exhibit enhanced catalytic and photocatalytic.[24,25] Though these procedures are effective, each design strategy alone always leads to limited improvement in the photocatalytic properties. And thus, the development of a facile, scalable and controllable fabrication of durable hybrid CeO_2 based materials with satisfactory photocatalytic performance is still highly desired, to our best knowledge, reports on the fast synthesis of hollow cubic TiO_2@CeO_2 heterostructures are quite rare compared with current methods that produced nanostructure, and can be an advantage for chemists to elaborate possible new constructions from all chemical components without any time-restricted conditions.

Herein, we chose coupled TiO_2@CeO_2 composites to demonstrate our concept and propose a facile fast strategy to prepare hollow nanocubic heterostructures with a high purity, high surface areas, and enhanced photocatalytic activity on detoxification of cyanide as illustrated in Scheme 1. The as-prepared Cu_2O nanocube is hired as the template, and then $S_2O_3^{2-}$ is used to self-gather around and coordinating etching of Cu_2O. Subsequently, OH^- originated from hydrolysis of $S_2O_3^{2-}$ results of the precipitation of Ti and Ce ions, and thus ($TiCe_x$)O(OH) precursor formed. Finally, thermal treatment facilitates the products of hollow TiO_2-CeO_2 nanocubes.

Compared with conventional template-assisted methods produced CeO_2 and TiO_2 materials, hollow-shaped TiO_2@CeO_2 hybrid nanoparticle aggregates prepared as such having relatively lower density, higher surface area and more stable hollow configuration without the destructive effect of template removal on product morphology. The heterojunction effect can lead to enhanced charge separation and interfacial charge transfer efficiency due to the existence of an internal electric field. Moreover, the hollow cubic structure can make a more efficient use of the light source via multiple reflections within the interior cavity. To our best knowledge, the fabrication of hollow TiO_2@CeO_2 hybrid nanocubes, which make an effective heterojunction between CeO_2 and TiO_2, has never been reported previously. Hence, a higher degree of metal utilization as enhanced detoxification of cyanide and degradation of dye under visible light can be expected.

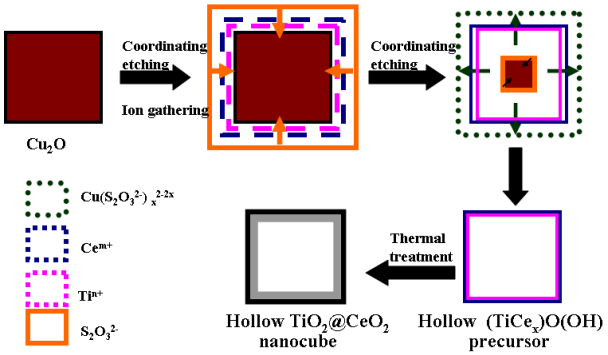

Scheme 1. Representative illustration of the formation of hollow TiO_2@CeO_2 nanocubes by simultaneous coordinating etching of Cu_2O nanocubes.

The whole fabrication process and experimental section of the hollow TiO_2@CeO_2 nanocubes are listed in ESI†. The SEM image and XRD pattern of as-prepared Cu_2O nanocubes are shown in Fig. 1a and b, showing cuprite structure Cu_2O (JCPDS card no. 77-0199) cubes.

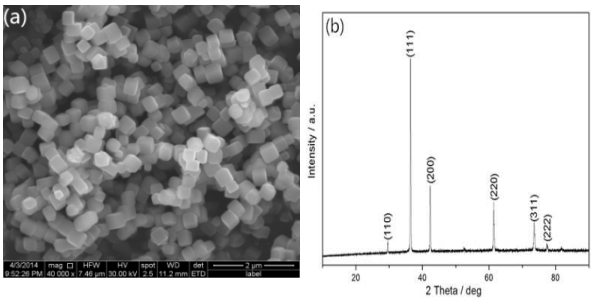

Fig. 1 SEM image (a) and XRD pattern (b) of prepared Cu_2O nanocubes.

The XRD patterns of the synthesized, ring-shaped TiO_2@CeO_2 hybrid nanoparticle aggregates and its precursor, shown in Fig. 2a, declare the product after calcinations at 450 °C exhibits higher crystallinity than that of $TiCe_xO(OH)$ precursor. The synthesized samples display composite materials corresponding to cubic fluorite-type CeO_2 (JCPDS card No. 81-0792) and tetragonal anatase TiO_2 structure (JCPDS card No. 21-1272). Detailed analysis of the peak broadening of the (1 1 1) reflection of TiO_2 using the Scherrer equation indicates an average crystallite size c.a. 5 nm, suggesting the particles are composed of nanocrystal subunits. The FTIR spectrum images of the prepared hollow nanocubes and that of the precursor are shown in Fig. 2b. The broad absorption peaks centered at ca. 3381 is associated with the asymmetric and symmetric stretching vibrations of the -OH group of absorbed water molecules, and that at 1572 cm^{-1} is assigned to the bending vibrations of the water molecules. The broad absorption peaks ranged of 500-1000 cm^{-1} are assigned to metal-O bond. The peak intensity of metal-O bond for the sample is different from that of precursor, implying the structure of prepared sample has a little discrepancy with its precursor. For the precursor, the weak peaks of 1402 cm^{-1} originated from the residual carbon species. This peak disappeared in the spectrum of synthesized final samples, indicating these organic groups have decomposed after calcinations. The strongest broad peaks in the range of 450-1100 cm^{-1} are contributed from the metal-oxide. The peak intensity is different from that of precursor, implying the structure of prepared sample has a little discrepancy with its precursor.

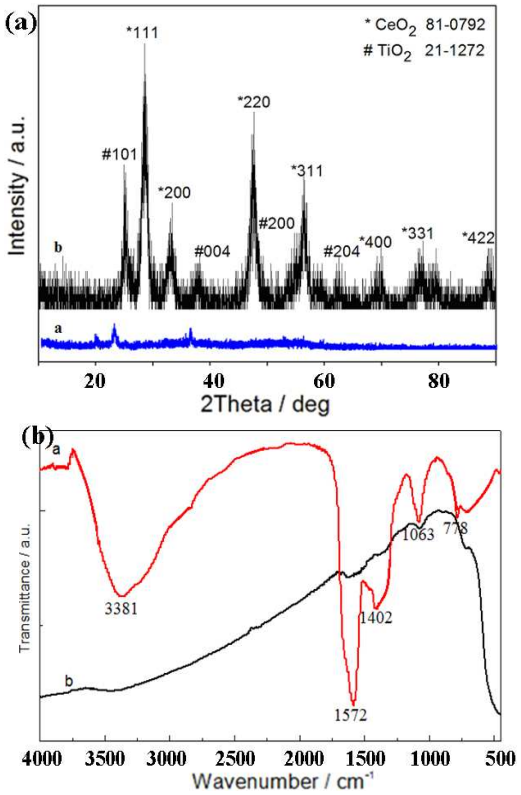

Fig. 2 (a) XRD pattern and FTIR spectra (b) of TiO_2@CeO_2 hybrid nanocubes and its precursor corresponding to curve a and b, respectively.

SEM images of the hybrid nanocubes of TiO_2@CeO_2 yielded by calcinations at 450 °C are shown as Fig. 3a and b. It is obvious that the synthesized fianal samples maintain the morphology of prepared Cu_2O except for a little shrinkage in size ca. 400 nm uniformly according to Fig. 3a. The obtained product is not a solid ball but a hollow cubic microstructure characteristic. Observation on part particles with partially broken shell, as shown in Fig. 3b indicates that the thickness of shell is estimated to ca. 30-50 nm and the surface of the synthesized powder is made up from nano-sized small particles. The cleft of these nanoboxes might be caused by rapid mass-transport across the shells during fast dissolution of the Cu_2O. The unique hollow crossed morphology of TiO_2@CeO_2 nanocube is also characterized by TEM and HR-TEM, as illustrated in Fig. 3c-f.

The low-magnification TEM image in Fig. 3c-d shows a hollow crossed nanocube, which is a visible hollow interior structure obviously. Especially, a typical nanobox with well-defined interior and very thin shell can be detected as Fig. 3d, which is in good agreement with SEM analysis. The thin thickness of shell of nanocubes is ca. 40 nm. This structure is almost the same as the expected model shown in Scheme 1. The selected area electron diffraction (SAED) pattern is displayed in Fig. 2e, which clearly reveals the presence of cubic fluorite-type CeO_2 and anatase TiO_2 structure. The (2 2 0) and (3 1 1) planes of cubic CeO_2, and (1 0 1) plane of anatase TiO_2 structure are seen through their interplanner spacing. Moreover, the detected lattice spacing of 0.353 nm and 0.192 nm agree with TiO_2 (1 0 1) and CeO_2 (2 2 0) plane spacing, respectively. These results are in total agreement with the observed XRD analysis. The unique cubic TiO_2@CeO_2 heterojunction is expected to be favorable for enhanced catalytic activity for detoxification of cyanide.

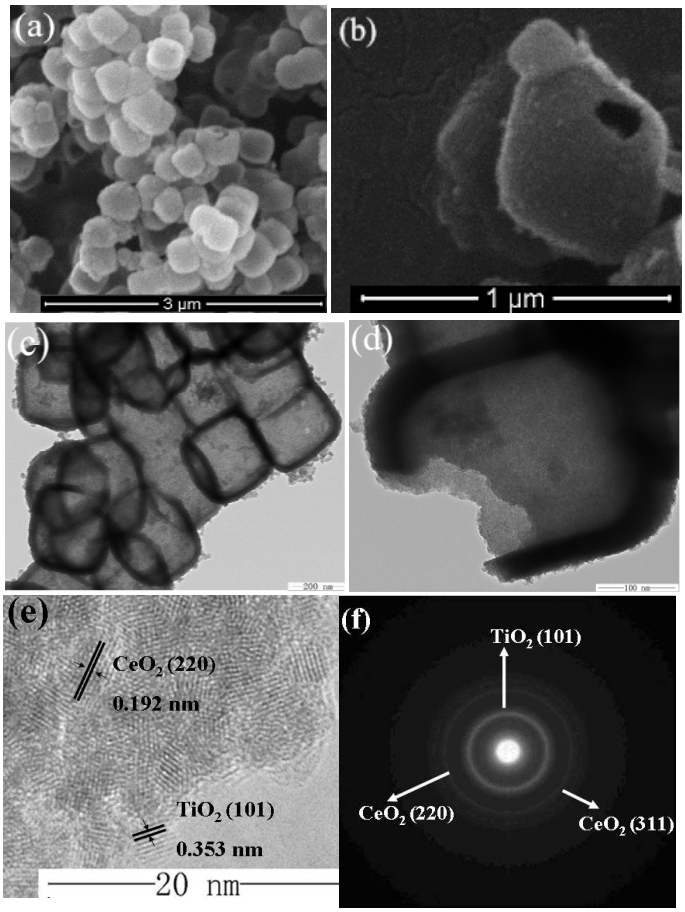

Fig. 3 SEM (a, b), TEM (c-d) images, HR-TEM micrographs (e) and (f) are the energy-dispersive X-ray spectroscopy (EDX) image and the selected area electron diffraction (SAED) of as-synthesized hollow nanocube 1 wt.% TiO_2/CeO_2 sample at different magnifications .

The BET surface area of the sample is 136.52 m^2g^{-1} (seeing Fig. S1a). The room temperature UV-vis absorption spectrum of the ample exhibits a wide visible-light absorption in the range of 400−550 nm (seeing Fig. S2a). We adopt the synthesis of CeO_2 to analyze the formation mechanism of hollow nanocubes, which can be described as schematically illustrated in Scheme 1 by the following formula:

$$Cu_2O + XS_2O_3^{2-} + H_2O \longrightarrow [Cu_2(S_2O_3)_x]^{2-2x} + 2OH^- \quad (1)$$

$$S_2O_3^{2-} + H_2O \longleftrightarrow HS_2O_3^- + OH^- \quad (2)$$

$$2xCe^{3+} + 2OH^- + O_2 \longrightarrow 2Ce_xO(OH) \quad (3)$$

$$Ce_xO(OH) \longrightarrow CeO_2 + H_2O \quad (4)$$

Firstly, coordinating etching reaction of $S_2O_3^{2-}$ to Cu_2O nanocubes was taken place under ambient conditions from its out to core, and offered OH^- as Equation 1. At the same time, those OH^- originated from hydrolysis of excess $S_2O_3^{2-}$ (Equation 2) can make the precipitation of Ce ions (Equation 3). And thus the Ce^{3+} around with etching interface of Cu_2O are self-gather and precipitate in aqueous solution with high concentration of OH^-, which process results in the formation of the shell of amorphous $Ce_xO(OH)$ precursor. The shell of $Ce_xO(OH)$ potentially thickens according to the concentration of Ce ions with the proceeding of reaction as Equation 3. It is interesting that the dissolution process of Cu_2O also undergoes even the $Ce_xO(OH)$ shell fully forms. The process is tracked to investigate the formation mechanism according to Fig. 4a-f, which is SEM image of simultaneous coordinating etching Cu_2O nanocubes at room temperature from 0 to 180 min. It is found clearly that nanocube structures can be detected initially (Fig. 4a). While the reaction is conducted for 30 min (Fig. 4b), the surface of sample becomes a little coarse and was transformed into hollow ones gradually. With the increase of reaction time (Fig. 4c, 90 min), the hollow structures become more significant. Further prolonging the reaction time, the interior of the nanocubes change empty as shown in Fig. 4d (120 min) and Fig. 4e (150 min). Finally, the hollow nanocubes are broken gradually, such as Fig. 4f (180 min). This dynamic process is different from the traditional concept of the sacrificial-template. Finally, CeO_2 hollow nanoboxes are obtained by thermal-induced dehydration of $Ce_xO(OH)$ (Equation 4), after annealing in Ar atmosphere. Compared with other reported CeO_2 based materials[26-29], our strategy provides a novel route to prepare hollow nanocubes with shorter time, more larger quantity and lower cost. This route can also be used to prepare other cage-bell advanced materials, such as TiO_2 (Fig. S2) and NiO (Fig. S3), for details see in supporting information**.**

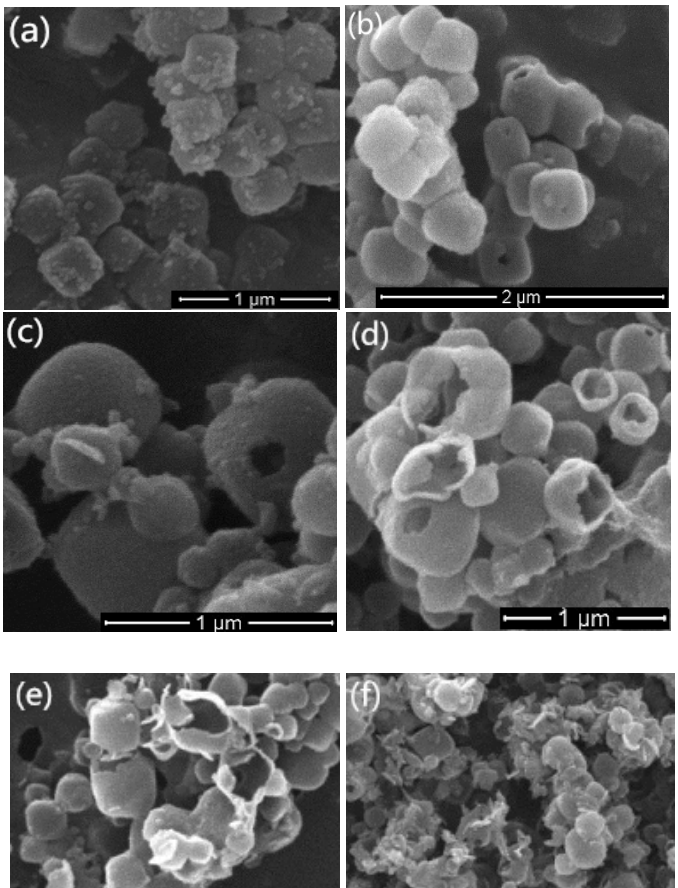

Fig. 4 SEM images of CeO_2 precursors by simultaneous coordinating etching of Cu_2O nanocubes at room temperature for 0 min (a), 30 min (b), 90 min (c), 120 min (d), 150 min (e) and 180 min (f).

Cyanide ion is not degraded under illumination in the absence of photocatalyst, nor in the dark in the presence of the photocatalyst. The time profiles of cyanide oxidation catalyzed TiO_2@CeO_2 hybrid materials under visible light are shown as Fig. 5, implying a steady and continuous degradation of the cyanide ion. The concentration of cyanide ion decreased sharply from the initial 4.70 mM to 0.18 mM corresponding to the removal rate of 96.17% with the exposure time in 90 min. However, the commercial CeO_2 and P25 (TiO_2) have not significant effect. The hollow cubic structures make multiple reflections of light within the chamber, allowing more efficient use of the light source. Moreover, the heterojunction effect can lead to enhanced charge separation and interfacial charge transfer efficiency. All the factors contribute greatly to the improved visible light catalytic activity. Compared with the other reports [7-11, 22, 30, 31], our strategy provides a novel route to prepare cube-shaped hybrid materials with higher effeciency for photocatalytic detoxification of cyanide.

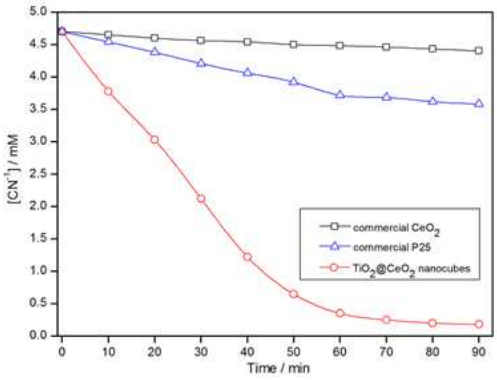

Fig. 5 Photodecomposition results: comparison of detoxification of cyanide in the presence of commercial P25 and CeO_2. pH = 12.5, catalyst loading = 0.02 g, airflow rate = 8.5 mL s^{-1}, $[O_2]_{dissolved}$ = 28.8 ppm.

In summary, hollow TiO_2@CeO_2 hybrid nanocubes are successfully synthesized by a facile and fast benign procedure by a simple simultaneous coordinated etching reaction and subsequent calcinations. It exhibits a remarkable activity for photocatalytic detoxification of cyanide. This strategy is simple, cheap and mass-productive, which may shed light on a new avenue for large-scale synthesis of hollow cube-shaped structural nano/micro functional hybrid materials for catalyst, energy and other applications.

The authors would like to acknowledge financial support provided by the National Natural Science Foundation of China (No.51474191 and No.21467030) and the Natural Science Foundation of Yunnan Province (No. 2014FB103).

Notes and references

School of Chemistry Science and Engineering, Yunnan University, Kunming 650091,Yunnan, China. Fax: +86-871-65036626; Tel: +86-871-65032180; E-mail: guohongcom@126.com

Electronic Supplementary Information (ESI) available: [details of any supplementary information available should be included here]. See DOI: 10.1039/b000000x/

1 R.R. Dash, C. Balomajumder and A. Kumar, *J. Chem. Eng.,* 2009, **146** 408.
2 J. Ma and P.K. Dasgupta, *Anal. Chim. Acta,* 2010, **673**, 117.
3 J.N.Smith, A.Keil, J. Likens and R.G. NollCooks, *Analyst,* 2010, **135**, 994.
4 R.R. Dash, A. Gaur and G. J. *Hazard. Mater*., 2009,**163,** 1.
5 R. C. Rocha-e-Silva, L. A. V. Cordeiro and B. Soto-Blanco, *Comp. Biochem. Phys. C*, 2010, **151**, 294.
6 M. Banea, G. Nahimana, C. Mandombi, J. H. Bradbury, I. C. Denton and N. Kuwa, *Food Chem. Toxicl.,* 2012, **50**, 1517.
7 J. Marugan, R.V. Grieken, A.E. Cassano and O.M. Alfano, *Catal. Today,* 2009, **144**, 87.
8 J. Marugan, R.V. Grieken, A.E. Cassano and O.M. Alfano, *Appl. Catal. B,* 2008, **85**, 48.
9 H. Guo, D. Tian, L. Liu, Y. Wang, Y. Guo and X. Yang, *J. Solid State Chem*., 2013, *201*,137.
10 A. Bozzi, I. Guasaquillo and J. Kiwi, *Appl. Catal. B,* 2004, **51**, 203.
11 F, Mou, L, Xu, H, Ma, J, Guan, D, Chen and S,Wang, *Nanoscale,* 2012, **4**, 4650.
12 L.S. Zhang, K.H. Wong, Z.G. Chen, J. C.Yu, J. C. Zhao, C. Hu, C. Y.Chan and P. K. Wong, *Appl. Catal., A*, 2009, **363**, 221.
13 M. C. Long, W. M. Cai, J. Cai, B. X. Zhou, X. Y. Chai and Y. H. Wu, *J. Phys. Chem. B*, 2006, **110**, 820211.
14 S. Y. Chai, Y. J. Kim, M. H. Jung, A. K. Chakraborty, D. Jung and W. I. Lee, *J. Catal.*, 2009, **262**, 144.
15 Y. Bessekhouad, D. Robert and J.-V. Weber, *J. Photochem. Photobiol. A*, 2004, **163**, 569.
16 J. Tian, Y. Sang, G. Yu, H. Jiang, X. Mu and H. Liu, *Adv. Mater.*, 2013, **25**, 5075.
17 J. Tian, Y. Sang, Z. Zhao, W. Zhou, D. Wang, X. Kang, H. Liu, J. Wang, S. Chen, H. Cai and H. Huang, *Small*, 2013, **9**, 3864.
18 X. Lu, L. Yang, X. Bian, D. Chao and C. Wang, Part. Part. Syst. Charact., 2014, **31**, 245.
19 J. Xie, D. Jiang, M. Chen, D. Li, J. Zhu, X. Lu, C.Yan, *Colloids Surf., A*, 2010, **372**, 107.
20 Y. Liu, P. Fang, Y. Cheng, Y. Gao, F. Chen, Z. Liu, Y. Dai, *Chem. Eng. J.* 2013, **219**, 478.
21 Z. F. Bian, J. Zhu, J. G. Wang, S. X. Xiao, C. Nuckolls and H. X. Li, *J. Am. Chem. Soc.,* 2012, **134**, 2325.
22 C. Karunakaran and P. Gomathisankar, *ACS Sustainable Chem. Eng.* 2013, 1, 1555.
23 H. Gnayem and Y. Sasson, *ACS Catal.*, 2013, **3**, 186
24 H. Guo, W. Wang, L. Liu, Y. He, C. Li and Y. Wang. *Green Chem.*, 2013, **15**, 2810.
25 H. Guo, Y. He, Y. Wang, L. Liu, X. Yang, S. Wang, Z. Huang and Q. Wei, J. Mater. Chem. A, 2013, 1, 7494.
26 R.V. Gulyaev, A.I. Stadnichenko, E.M. Slavinskaya, A.S. Ivanova, S.V. Koscheev and A.I. Boronin, *Appl. Catal. A-Gen.,* 2012*,* **439**, 41.
27 L. Q. Liu, F. Zhou, L. G. Wang, X. J. Qi, F. Shi and Y. Q. Deng, *J. Catal.,* 2010, **274**, 1.
28 Y. S. Bi, L. Chen and G. X. Lu, *J. Mol. Catal. A-Chem.,* 2007, **266**, 173.
29 L. L. Cai, G. Z. Lu, W. C. Zhan, Y. Guo, Y. L. Guo, Q. S. Yang and Z. G. Zhang, *J. Mater. Sci.,* 2011, **46**, 5639.
30 F, Mou, C, Chen, J, Guan, D, Chen and H, Jing, *Nanoscale,* 2013, **5**, 2055.
31 J. R. Parga, V. Vázquez, H. M. Casillas and J. L. Valenzuela, *Chem. Eng. Technol.*, 2009, **32**, 1901.

